Adaptive Array Processing for Multipath Fading Mitigation via Exploitation of Filter Banks

Yimin Zhang, *Member, IEEE*, Kehu Yang, *Member, IEEE*, and Moeness G. Amin, *Fellow, IEEE*

Abstract—In this paper, we propose subband adaptive array processing for mitigation of both intersymbol interference (ISI) and cochannel interference (CCI) in digital mobile communications. Subband adaptive array processing employs filter banks in a front end to an adaptive array receiver. By decomposing the signals into a set of subband signals, the analysis filters enhance the correlation of multipath rays in each subband. This enhancement is blind in the sense that no *a priori* knowledge of the temporal characteristics or spatial signatures of arriving signals is required. With the increased coherence, the desired signal can be effectively equalized by subsequent spatial processing. Further, the CCI signals and their multipaths can be suppressed with fewer degrees of freedom. The effects of quadrature mirror filter and discrete Fourier transform filter banks on multipath correlation are delineated.

Index Terms—Adaptive arrays, fading channels, filter banks, multipath channels, space–time adaptive processing.

I. INTRODUCTION

IN LAND mobile communications, a user signal transmitted by a mobile station is reflected and scattered by surroundings before arriving at a base station, creating a multipath fading problem. As the demand for multimedia communications is increasing, mobile communication technology is developing toward high-speed digital wireless networks, where the communication channels are frequency selective and the intersymbol interference (ISI) is highly pronounced. Another source of channel distortion and signal impairment is cochannel interference (CCI), which is generated due to frequency reuse in cellular systems.

Adaptive arrays implementing spatial or spatial-temporal equalizations have shown to be effective in suppressing both ISI and CCI, leading to increased capacity and range [1]–[8]. Spatial-temporal equalizations can be achieved by space-time adaptive processing (STAP), which is composed of an integrated adaptive array and temporal filters. However, solving both the CCI and the ISI problems simultaneously by conventional STAP methods remains difficult, as these methods require either large-scale matrix inversion or recursive computation, or a cascaded form of CCI and ISI cancellers [6]–[8].

In this paper, we propose an efficient subband adaptive array processing method that utilizes filter banks to mitigate both the CCI and the ISI effects in land mobile communications [9]. A subband adaptive array is suboptimum in the context of spatial-spectral signal processing. It achieves the same objective as a STAP system, while the implementation is more effective. With subband decomposition, the problem is converted into a number of simple spatial equalizations that could be performed in parallel. In subband adaptive arrays, the frequency band of the received signals is divided into smaller subbands by the use of filter banks [10]. Proper analysis filters allow a significant increase in the signal correlation between the multipath rays within each subband. As a result of increased correlation, the effect of multipath fading associated with both the desired and the interference signals is reduced, and, as such, fewer degrees of freedom (DOFs) are required for proper equalization and CCI suppression [9], [11]. Note that such an increase of the signal correlation is blind in the sense that it does not require *a priori* knowledge of the temporal characteristics or spatial signatures of the signals incident in the array. Therefore, this method can be easily extended to realize blind space–time adaptive processing [12].

Subband adaptive array methods have been proposed for wide-band signal processing and are known to offer the advantages of reduced processing rates [13] and rapid convergence [14], [15]. The coherent subspace transformation methods [16], [17] also demonstrate these two advantages.

In this paper, the discussion of subband signal processing is mainly focused on the signal correlation enhancement in a frequency-selective fading environment, rather than the conventional consideration of reducing the signal bandwidth and the computational complexity. Subband processing, in essence, converts a frequency-selective fading problem into a flat fading problem. As a result, the ISI can be effectively mitigated, as the faded signal can be equalized by a subsequent spatial combiner. Since the CCI components in each subband are easily removed by the respective narrow-band adaptive array, subband adaptive array techniques can simply solve both CCI and ISI problems simultaneously.

Although many transformation methods can convert a wide-band signal into multiple-channel narrow-band signals, it is shown in this paper that different methods provide different signal correlation enhancements, and, therefore, lead to a different receiver performance. The importance of the proper selection of the analysis and synthesis filters to obtain good equalization performance by subband signal processing is emphasized.

Y. Zhang was with the ATR Adaptive Communication Research Laboratories, Kyoto 619-0288 Japan. He is now with the Department of Electrical and Computer Engineering, Villanova University, Villanova, PA 19085 USA (e-mail: yimin@ieee.org).

K. Yang was with the Institute of Electronics Engineering, Xidian University, Xi'an, Shaanxi, China. He is now with the ATR Adaptive Communication Research Laboratories, Kyoto 619-0288, Japan (e-mail: yang@acr.atr.co.jp).

M. G. Amin is with Department of Electrical and Computer Engineering, Villanova University, Villanova, PA 19085 USA (e-mail: moeness@ece.vill.edu).
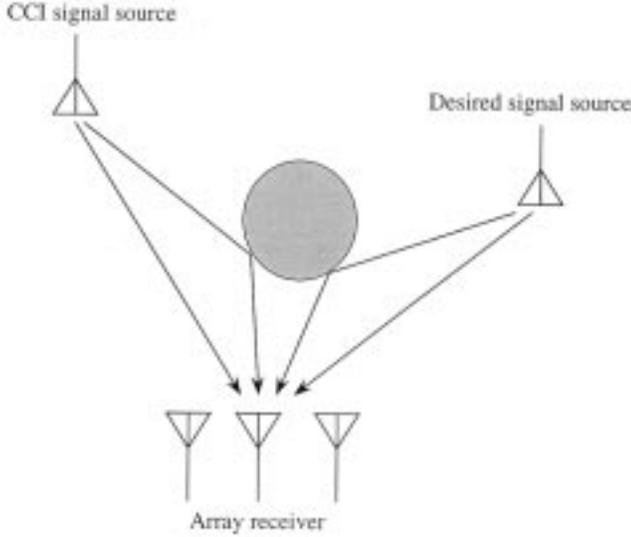
Fig. 1.   Multipath environment.

This paper is organized as follows. In Section II, we first present the framework of adaptive array processing in the presence of multipath rays. It is shown that multipath rays of a signal can be treated as a single ray when their cross-correlation is relatively high. In Section III, different filter banks are analyzed and compared in terms of the enhancement of the signal correlation between multipath signals. The analysis of the subband array performance is given in Section IV. In Section V, simulation examples are provided to illustrate the effectiveness of the proposed method.

II. ADAPTIVE ARRAY FRAMEWORK IN THE PRESENCE OF MULTIPATH RAYS

Without loss of generality, we consider the simple case where a desired signal and a CCI component, each with two rays, are incident on an array of N sensors, as shown in Fig. 1. The received array vector is described as

$$\mathbf{x}(t) = \mathbf{A}(\Theta_D)\mathbf{s}_D(t) + \mathbf{A}(\Theta_I)\mathbf{s}_I(t) + \mathbf{n}(t) \qquad (1)$$

where

$\mathbf{A}(\Theta_D) = [\mathbf{a}(\theta_{D1}), \mathbf{a}(\theta_{D2})]$ array manifold matrix, which is the collection of the two steering vectors for the desired signal;

$\mathbf{s}_D(t) = [s_{D1}(t), s_{D2}(t)]^T$ vector that includes the respective complex envelopes at the presumed phase reference point of the array;

$\mathbf{A}(\Theta_I) = [\mathbf{a}(\theta_{I1}), \mathbf{a}(\theta_{I2})]$;   corresponding array manifold
$\mathbf{s}_I(t) = [s_{I1}(t), s_{I2}(t)]^T$ matrix and complex envelop vector for the CCI signal.

It is assumed that the desired signal and the CCI signal are independent. We also assume that the elements of the noise vector $\mathbf{n}(t)$ are independent and identically distributed (i.i.d.) Gaussian random processes with zero-mean and covariance matrix $\sigma_N^2 \mathbf{I}$, where $\mathbf{I}$ is the $N \times N$ identity matrix. $s_{D1}(t)$ is used to represent the direct ray and is considered as the signal of interest (SOI).

The multipath ray $s_{D2}(t)$ of the desired signal can be decomposed into two components: one is coherent with the SOI and the other is orthogonal to the SOI [18], i.e.,

$$s_{D2}(t) = \rho_D^* \xi_D s_{D1}(t) + s_D^\perp(t) \qquad (2)$$

where $E[s_D^\perp(t) s_{D1}(t)] = 0$ and

$$\rho_D = \frac{E[s_{D1}(t) s_{D2}^*(t)]}{\sigma_{D1}\sigma_{D2}} \qquad (3)$$

is the signal correlation between the two rays whose power are σ_D^2 ($\overset{\triangle}{=} \sigma_{D1}^2$) and σ_{D2}^2, respectively, and $\xi_D = \sigma_{D2}/\sigma_{D1}$. $E[\cdot]$ represents the expectation operator and $(\cdot)^*$ denotes complex conjugation. The signal correlation matrix is defined as

$$\mathbf{R}'_{DD} = E\left[\mathbf{s}_D(t)\mathbf{s}_D^H(t)\right]$$
$$= \sigma_D^2 \begin{bmatrix} 1 & \rho_D\xi_D \\ \rho_D^*\xi_D & |\rho_D\xi_D|^2 \end{bmatrix} + \begin{bmatrix} 0 & 0 \\ 0 & (1-|\rho_D|^2)\sigma_{D2}^2 \end{bmatrix} \qquad (4)$$

where $(\cdot)^H$ denotes complex conjugate transpose. Accordingly, the spatial correlation matrix is given by

$$\mathbf{R}_{DD} = \mathbf{A}(\Theta_D) E\left[\mathbf{s}_D(t)\mathbf{s}_D^H(t)\right] \mathbf{A}^H(\Theta_D)$$
$$= [\mathbf{a}(\theta_{D1}), \mathbf{a}(\theta_{D2})]\left\{\sigma_D^2 \begin{bmatrix} 1 & \rho_D\xi_D \\ \rho_D^*\xi_D & |\rho_D\xi_D|^2 \end{bmatrix}\right.$$
$$\left. + \begin{bmatrix} 0 & 0 \\ 0 & (1-|\rho_D|^2)\sigma_{D2}^2 \end{bmatrix}\right\} \begin{bmatrix} \mathbf{a}(\theta_{D1}) \\ \mathbf{a}(\theta_{D2}) \end{bmatrix}$$
$$= \sigma_D^2[\mathbf{a}(\theta_{D1}) + \rho_D^*\xi_D\mathbf{a}(\theta_{D2})]$$
$$\times [\mathbf{a}(\theta_{D1}) + \rho_D^*\xi_D\mathbf{a}(\theta_{D2})]^H$$
$$+ (1-|\rho_D|^2)\sigma_{D2}^2\mathbf{a}(\theta_{D2})\mathbf{a}^H(\theta_{D2}) \qquad (5)$$

The first term of the right-hand side of (5) is constructed from the combined signal vector $\tilde{\mathbf{s}}_D(t) = [\mathbf{a}(\theta_{D1}) + \rho_D^*\xi_D\mathbf{a}(\theta_{D2})]s_{D1}(t)$, where the quantity in the brackets

$$\tilde{\mathbf{a}}_D = \mathbf{a}(\theta_{D1}) + \rho_D^*\xi_D\mathbf{a}(\theta_{D2}) \qquad (6)$$

represents the generalized steering vector of the SOI. The second term in (5) is the contribution to the ISI from the orthogonal components $s_D^\perp(t)$. This contribution vanishes asymptotically as $|\rho_D|$ approaches one.

By assuming that the reference signal $r(t)$ is an ideal replica of the SOI $s_{D1}(t)$, then the correlation vector between the data vector $\mathbf{x}(t)$ and the reference signal $r(t)$ is

$$\mathbf{r}_D = E[\mathbf{x}(t)r^*(t)] = E[\mathbf{x}(t)s_{D1}^*(t)] = \sigma_D^2\tilde{\mathbf{a}}_D \qquad (7)$$

which coincides with the generalized steering vector of the SOI, given in (6). Thus, the optimum weight vector under the minimum mean-square error (MMSE) criterion is given by [19]

$$\mathbf{w} = \mathbf{R}_{XX}^{-1}\mathbf{r}_D = g\mathbf{R}_N^{-1}\tilde{\mathbf{a}}_D \qquad (8)$$

where $g = \sigma_D^2(1 - \sigma_D^2\tilde{\mathbf{a}}_D^H\mathbf{R}_{XX}^{-1}\tilde{\mathbf{a}}_D)$ is a constant and

$$\mathbf{R}_{XX} = E[\mathbf{x}(t)\mathbf{x}^H(t)] = \mathbf{R}_N + \sigma_D^2\tilde{\mathbf{a}}_D\tilde{\mathbf{a}}_D^H, \qquad (9)$$
$$\mathbf{R}_N = (1 - |\rho_D|^2)\sigma_{D2}^2\mathbf{a}(\theta_{D2})\mathbf{a}^H(\theta_{D2}) + \mathbf{R}_{IN}. \qquad (10)$$

$\mathbf{R}_N$ is the equivalent correlation matrix of all interfering and undesired components and

$$\mathbf{R}_{IN} = \mathbf{R}_{II} + E[\mathbf{n}(t)\mathbf{n}^H(t)] = \mathbf{R}_{II} + \sigma_N^2 \mathbf{I}. \quad (11)$$

$\mathbf{R}_{II}$ is the correlation matrix of the CCI signal vector, which is defined in (14). By using the matrix inversion formula, we obtain

$$\mathbf{R}_N^{-1} = \mathbf{R}_{IN}^{-1} - \varepsilon \mathbf{R}_{IN}^{-1} \mathbf{a}(\theta_{D2}) \mathbf{a}^H(\theta_{D2}) \mathbf{R}_{IN}^{-1} \quad (12)$$

where

$$\varepsilon = \frac{(1 - |\rho_D|^2)\sigma_{D2}^2}{1 + (1 - |\rho_D|^2)\sigma_{D2}^2 \mathbf{a}^H(\theta_{D2})\mathbf{R}_{IN}^{-1}\mathbf{a}(\theta_{D2})} \quad (13)$$

which monotonously decreases as $|\rho_D|$ increases.

From the above analysis, it is evident that the array weight vector $\mathbf{w}$ will be less influenced by the orthogonal component $s_D^\perp(t)$ as $|\rho_D|$ increases. When $|\rho_D|$ reaches the unit value, the two multipath rays become coherent and can be equivalently considered as a single ray. In this case, they can be handled by a single DOF. Consequently, the frequency-selective fading problem is converted into a flat fading problem, whereby the channel can be spatially equalized and the ISI issue is resolved. The employed spatial equalization scheme should also suppress all CCI components.

To examine the effect of signal correlation enhancement to the CCI components, we use eigendecomposition methods. The correlation matrix of the CCI signal vector, denoted by $\mathbf{R}_{II}$, can be expressed as

$$\mathbf{R}_{II} = \mathbf{A}(\Theta_I)E\left[\mathbf{s}_I(t)\mathbf{s}_I^H(t)\right]\mathbf{A}^H(\Theta_I) = \sum_{i=1}^{2} \lambda_{Ii}\mathbf{u}_{Ii}\mathbf{u}_{Ii}^H \quad (14)$$

where λ_{Ii} $(i = 1, 2)$ are the eigenvalues of $\mathbf{R}_{II}$ and $\mathbf{u}_{Ii}$ are the corresponding eigenvectors. The two eigenvalues are given by [20]

$$\lambda_{I1,2} = \frac{N}{2}\left[\sigma_{I1}^2 + \sigma_{I2}^2 + 2\sigma_{I1}\sigma_{I2}\,\mathrm{Re}(\rho_I\beta_I^*)\right]$$
$$\times \left[1 \pm \sqrt{1 - \frac{4\sigma_{I1}^2\sigma_{I2}^2(1 - |\beta_I|^2)(1 - |\rho_I|^2)}{[\sigma_{I1}^2 + \sigma_{I2}^2 + 2\sigma_{I1}\sigma_{I2}\,\mathrm{Re}(\rho_I\beta_I^*)]^2}}\right] \quad (15)$$

where

$\sigma_{I1}^2; \sigma_{I2}^2$ powers of the two rays of the CCI signal, respectively;

ρ_I signal temporal correlation coefficient between the two rays;

β_I their spatial correlation coefficient, defined as

$$\beta_I = \frac{\mathbf{a}^H(\theta_{I1})\mathbf{a}(\theta_{I2})}{||\mathbf{a}(\theta_{I1})||||\mathbf{a}(\theta_{I2})||^{1/2}} \quad (16)$$
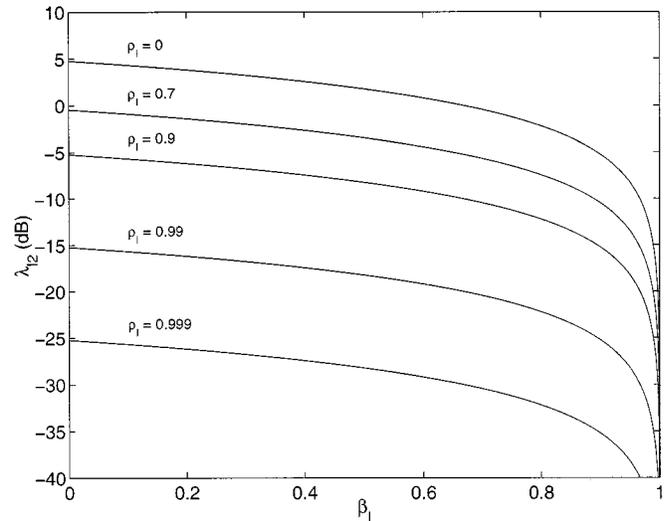
where $|| \ ||$ denotes the 2-norm of a vector.

Fig. 2. λ_{I2} versus ρ_I and β_I.

It is clear that λ_{I2} becomes zero when either or both of $|\rho_I|$ and $|\beta_I|$ become one. For these cases, the two rays behave as a single one. Therefore, while the array often needs two DOFs to effectively suppress two waveforms with low signal correlation, it suffices only to use a single DOF when the waveforms are highly correlated statistically and/or spatially.

In practice, the second eigenvalue λ_{I2} can be neglected when it is much smaller than the noise power σ_N^2, as either or both of $|\rho_I|$ and $|\beta_I|$ assume high value. In this case, the rank of the interference subspace is effectively one. It is evident from (15) that the required values of $|\rho_I|$ and $|\rho_I|$ to mitigate the ISI effect increase with higher SNR. Fig. 2 illustrates the second eigenvalue λ_{I2} as a function of ρ_I and β_I.

III. SIGNAL CORRELATION ENHANCEMENT USING FILTER BANKS

In the previous section, we discussed the adaptive array framework in the presence of frequency-selective multipath rays. It is shown that the increase of the correlation between signal multipath rays converts the frequency-selective problem into a flat fading problem, so that a signal can be equalized by only spatial processing. When this correlation is very high, the multipath rays can be treated as a single equivalent ray with a generalized steering vector. A generalized beam can then be formed to combine the multipath rays of the desired signal, consuming a single array DOF. Similarly, the multipath rays of each CCI signal will be suppressed by a single array DOF.

This section discusses the signal correlation enhancement of multipath rays by subband signal processing. We first briefly review the concept of subband signal processing using filter banks, then present the basic principle of coherency enhancement via subband partitioning via ideal filters. Next, we consider discrete Fourier transform (DFT) filter banks and quadrature mirror filter (QMF) banks as two examples to implement the subband signal processing, and the performances of signal correlation enhancement are compared. Polyphase filters are another member of filter banks, but are not considered herein.
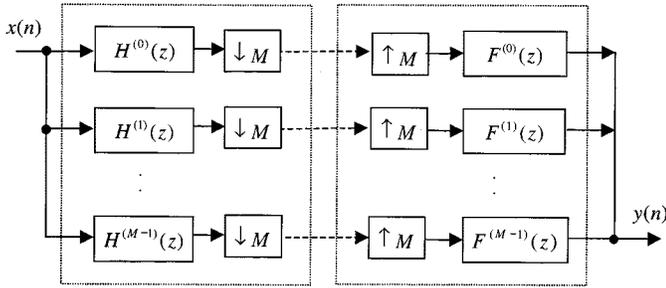
Fig. 3.   Block diagram of a filter bank.

Fig. 4.   Block diagram of a DFT filter bank.

A. Subband Signal Processing by Using Filter Banks

A filter bank is a set of filters linked by sampling operators and sometimes by delays. Fig. 3 shows the block diagram of a filter bank. The z-transform of the output $y(n)$ is expressed as

$$Y(z) = T(z)X(z) + \sum_{k=1}^{M-1} A_k(z)X(e^{j2\pi k/M}z) \qquad (17)$$

where $X(z)$ is the z-transform of $x(n)$

$$T(z) = \frac{1}{M} \sum_{k=1}^{M} H^{(k)}(z)F^{(k)}(z), \qquad (18)$$

$$A_k(z) = \frac{1}{M} \sum_{k=1}^{M} H^{(k)}(e^{-j2\pi k/M}z)F^{(k)}(z) \qquad (19)$$

and M is the number of subbands. We assume maximum decimation such that the decimation rate equals to M. The first term of the right side of (17) is the nonaliasing component, and the second term is the aliasing component. To realize the perfect reconstruction (PR) of the filter bank, it is required that

$$T(z) = z^{-n_0} \qquad (20)$$
$$A_k(z) = 0, \qquad \text{for } k = 1, 2, \ldots, M-1 \qquad (21)$$

where $n_0 > 0$ is an arbitrary integer.

Under the PR condition, the output of the filter bank is a delayed version of the input without distortion, i.e.,

$$y(n) = x(n - n_0). \qquad (22)$$

If a filter bank consists of M ideal bandpass filters, that is

$$H^{(k)}(f) = F^{(k)}(f)$$
$$= \begin{cases} 1, & -\frac{B}{2} + \frac{k-1}{M}B \le f < -\frac{B}{2} + \frac{k}{M}B \\ 0, & \text{elsewhere} \end{cases}$$
$$\qquad (23)$$

then clearly the filter bank satisfies the PR condition. Although such a filter bank is not causal, it provides simple expressions, which will be used to analyze the signal correlation enhancement in Section III-B.

Among the many filter bank implementations, DFT filter banks and QMF banks are used as examples to illustrate their performance of signal correlation enhancement and the comparison with the ideal filter banks. DFT filter banks, consisting of DFT and inverse DFT (IDFT) transforms, are shown in
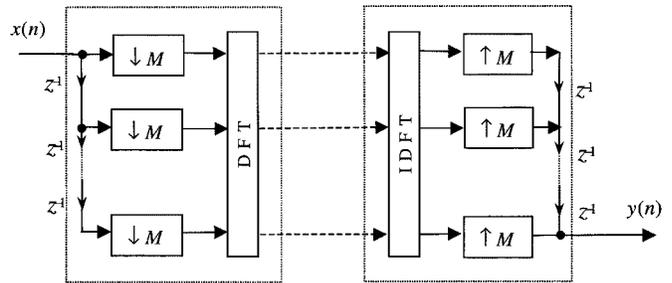
Fig. 4. The DFT filter bank is discussed in Section III-C. Fig. 5 shows the frequency responses of the ideal DFT and QMF filter banks.

QMF banks, or, more practically, pseudo-QMF banks, are often used to realize efficient subband signal processing with perfect or near-perfect reconstruction (NPR) [10], [21], [22]. A QMF bank has the same construction as the filter bank shown in Fig. 3, where in a QMF bank each of the analysis or synthesis filters can be realized by a finite impulse response (FIR) filter with finite taps. In a pseudo-QMF bank, the filter bank channels are formed by a series of equidistant frequency shifts of an appropriate prototype filter, and the transfer functions of adjacent channels are approximately power complementary between their center frequencies. The pseudo-QMF banks are discussed in Section III-D.

It is noted that with the use of the adaptive processing between the analysis filters and the synthesis filters, the subband processing system is no longer PR even when the original subband system is PR. In this case, the sidelobes of the subband filter system will cause aliasing, yielding less efficient signal correlation enhancement. The frequency responses of the three types of analysis filters are given in Fig. 5. The ideal filter banks do not have cross spectra, whereas the DFT filter banks have relatively high sidelobe level and cross spectra between different subbands. Their performance will be discussed in detail below.

B. Basic Principle of Coherency Enhancement via Subband Partition

Consider a bandlimited random signal $s(t)$. For the simplicity of analysis, we assume that the signal power spectrum density function (PSDF), denoted by $p(f)$, is flat within the bandwidth B, i.e.,

$$p(f) = \begin{cases} 1, & -\frac{B}{2} \le f \le \frac{B}{2} \\ 0, & \text{elsewhere} \end{cases} \qquad (24)$$

The corresponding autocorrelation function, denoted by $r(\tau)$, is obtained by the Fourier transform of $p(f)$ as

$$r(\tau) = E\{s(t)s^*(t - \tau)\} = \frac{\sin(\pi B\tau)}{\pi\tau} = B\,\text{sinc}(B\tau). \qquad (25)$$

If we equally partition $p(f)$ into M subbands, such as

$$p(f) = \sum_{k=0}^{M-1} p^{(k)}(f) \qquad (26)$$
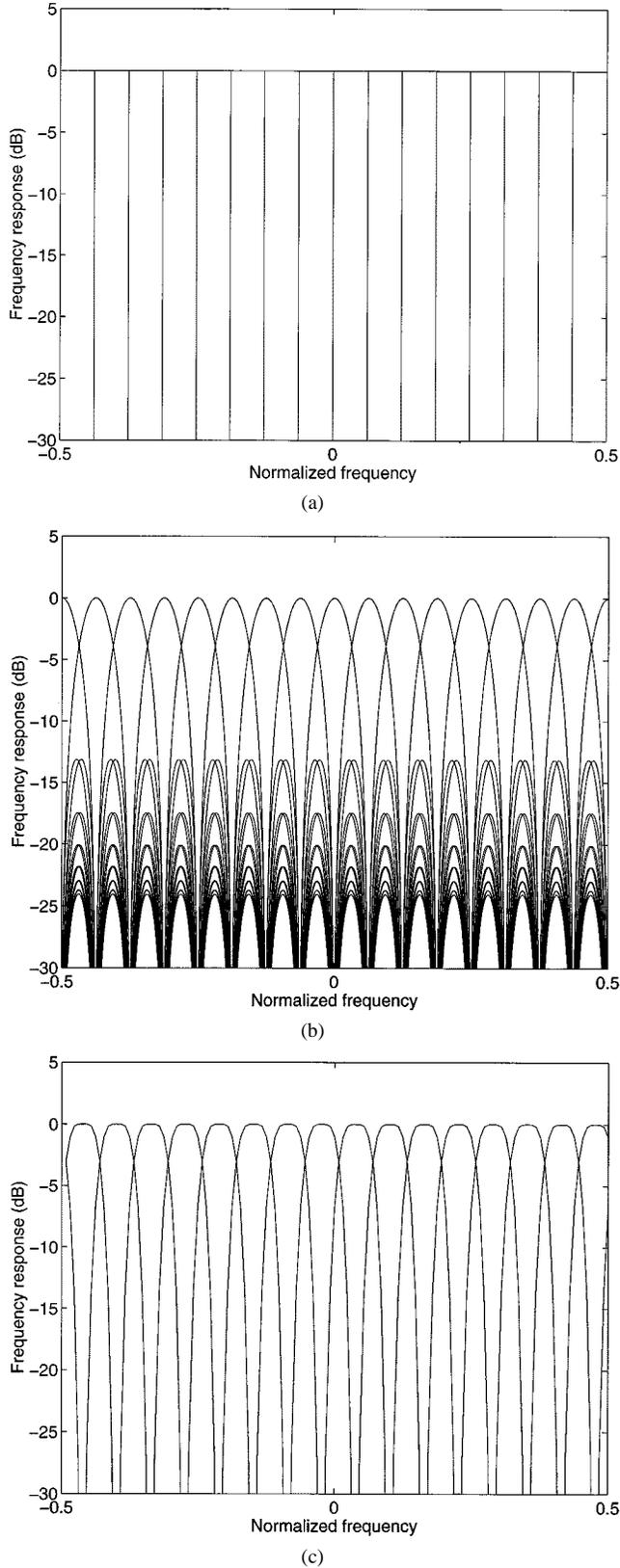
(a)

(b)

(c)

Fig. 5. Frequency response of different filter banks ($M = 16$). (a) Ideal filter bank. (b) DFT filter bank. (c) Modified QMF bank.

where

$$p^{(k)}(f) = \begin{cases} 1, & -\frac{B}{2} + \frac{k}{M} B \le f < -\frac{B}{2} + \frac{k+1}{M} B \\ 0, & \text{elsewhere} \end{cases} \tag{27}$$
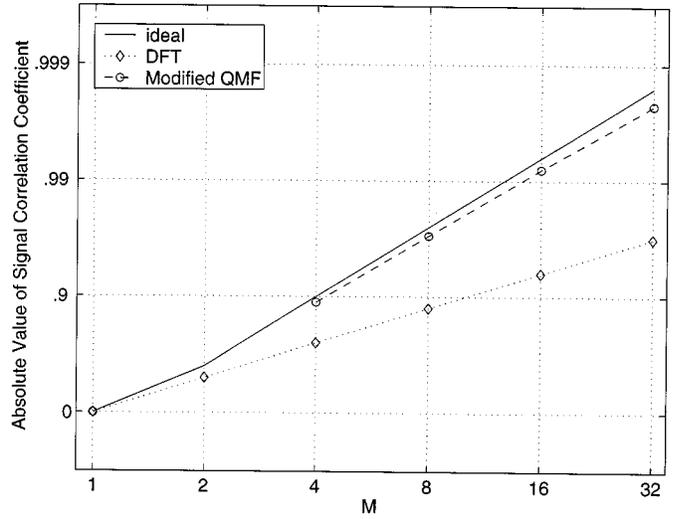

Fig. 6. Signal correlation coefficient versus M for $\tau = T_S$.

then the autocorrelation function for the kth subband signal $s^{(k)}(t)$ will be

$$r^{(k)}(\tau) = E\left\{s^{(k)}(t)s^{(k)^*}(t - \tau)\right\}$$

$$= \frac{\sin\left(\frac{\pi B \tau}{M}\right)}{\pi \tau} e^{j \frac{\pi B \tau}{M}(2k - M - 1)}$$

$$= \frac{B}{M} \operatorname{sinc}\left(\frac{B\tau}{M}\right) e^{j \frac{\pi B \tau}{M}(2k - M - 1)}. \tag{28}$$

The signal correlation coefficient of $s(t)$ and its delayed replica $s(t - \tau)$ is then

$$\rho(\tau) = \alpha \frac{r(\tau)}{r(0)} = \alpha \operatorname{sinc}(B\tau) \tag{29}$$

where α ($|\alpha| = 1$) is a factor used to express the propagation phase difference between $s(t)$ and $s(t - \tau)$. Similarly, for the kth subband signal, we have

$$\rho^{(k)}(\tau) = \alpha \frac{r^{(k)}(\tau)}{r^{(k)}(0)} = \alpha \operatorname{sinc}\left(\frac{B\tau}{M}\right) e^{j(2k - M - 1)\pi B \tau / M}. \tag{30}$$

By comparing (29) and (30), it becomes evident that the signal correlation coefficient of the subband signal is stretched M times over time. We note that $|\rho^{(k)}(\tau)|$ does not change with k, which implies that the signal correlation is equally enhanced for the different subbands. For example, when $\tau = 1/B$, we have $\rho(1/B) = 0$, which means that the two signals are uncorrelated. When the signal is divided into M subbands, then $|\rho^{(k)}(1/B)| = \operatorname{sinc}(1/M)$, which equals to 0.9936 for $M = 16$. Therefore, the two uncorrelated rays become approximately coherent in the subbands. The correlation $|\rho^{(k)}(\tau)|$ is plotted versus M and is shown by the solid line in Fig. 6 for $B\tau = 1$. It is noted that when τ is large, M should be sufficiently large such that $B\tau/M$ is much smaller than one.

C. Subband Partition via DFT Filter Banks

In Section III-B, we considered the filter bank based on ideal filters. However, for causal systems, the transfer function of an FIR filter does not have the shape of a rectangular pulse. Below,

we consider two types of filter banks, that is, DFT and QMF, for examples. In this section, we analyze the performance of signal correlation enhancement when DFT filter banks are used.

We consider the discrete form. The critical sampling is assumed, that is, the sampling period is $T_S = 1/B$. The DFT of a data sequence $x(n)$ is defined as

$$X(k) = \sum_{n=0}^{M-1} x(n)W^{nk}, \quad k = 0, 1, \ldots, M-1 \quad (31)$$

where $W = e^{-j2\pi/M}$. The kth subband output of the DFT is

$$y^{(k)}(l) = \sum_{n=0}^{M-1} x(l-n)e^{-j2\pi(M-1-n)k/M}$$
$$0 \leq k \leq M-1. \quad (32)$$

The impulse responses of kth subband DFT analysis and synthesis filter can be described as

$$\begin{cases} h_k(n) = e^{-j2\pi(M-1-n)k/M} \\ f_k(n) = e^{j2\pi nk/M} \end{cases}$$
$$0 \leq n \leq M-1, \quad 0 \leq k \leq M-1. \quad (33)$$

Then, the z-domain transfer functions of the filters are described as

$$\begin{cases} H_k(z) = \sum_{n=0}^{M-1} z^{-n} e^{-j2\pi(M-1-n)k/M} \\ F_k(z) = \sum_{n=0}^{M-1} z^{-n} e^{j2\pi nk/M} \end{cases}$$
$$0 \leq k \leq M-1 \quad (34)$$

respectively, and the frequency response of the kth analysis filter is

$$H^k(f) = \sum_{n=0}^{M-1} e^{-j2\pi nf/B} e^{-j2\pi(M-1-n)k/M}$$
$$= \frac{\sin(\pi M(f/B - k/M))}{\sin(\pi(f/B - k/M))} e^{-j\pi(M-1)(f/B - k/M)}. \quad (35)$$

Equation (35) has the form of Dirichlet kernel. From (35) and

$$p^{(k)}(f) = \left| H^{(k)}(f) \right|^2 p(f) \quad (36)$$

the autocorrelation function and signal correlation coefficient of the kth subband filter output signal are

$$r^{(k)}(\tau) = \int_{-\infty}^{\infty} p^{(k)}(f)e^{j2\pi f\tau} df$$
$$= \int_{-\infty}^{\infty} \sum_{n=0}^{M-1} \sum_{m=0}^{M-1} e^{-j2\pi f(n-m)/B}$$
$$\times e^{-j2\pi(m-n)k/M} p(f)e^{j2\pi f\tau} df$$
$$= \sum_{n=0}^{M-1} \sum_{m=0}^{M-1} e^{-j2\pi(m-n)k/M} r\left(\tau - \frac{n-m}{B}\right) \quad (37)$$

$$\rho^{(k)}(\tau) = \alpha r^{(k)}(\tau)/r^{(k)}(0). \quad (38)$$

The signal correlation coefficient is plotted in Fig. 7 for the different subbands. It is seen that the curve is flat only when
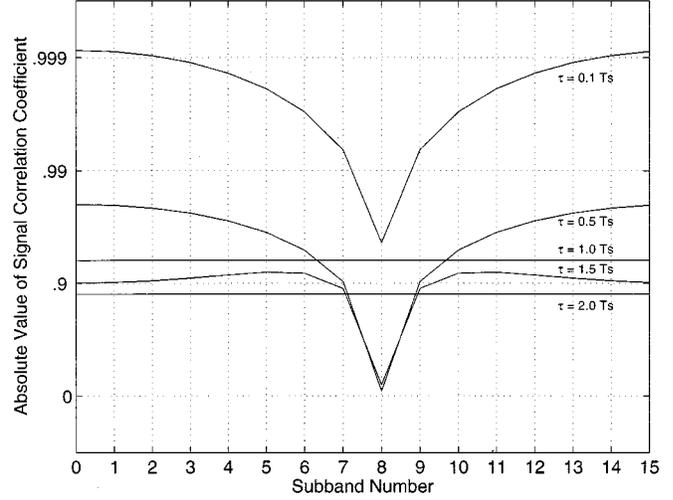

Fig. 7. Signal correlation coefficient of DFT filter banks at the different subbands ($M = 16$).

τ/T_S is an integer. In the other cases, the signal correlation coefficient has the largest value at $k = 0$, and the coefficient is very small at $k = M/2$, particularly when the modulo of τ/T_S is 0.5.

The correlation coefficient between the two rays is given as the dotted line in Fig. 6 for $B\tau = 1$ and $k = 0$. $|\rho^{(k)}(\tau)|$ is approximately 0.935 when $M = 16$. From Fig. 6, it is clear that the DFT filter banks provide meager signal correlation enhancement. Thus, filter banks with more powerful correlation enhancement are preferable to reduce the number of subband partitions.

D. Subband Partition via QMF Banks

We now discuss the signal correlation enhancement using pseudo QMF banks. The impulse responses of the pseudo-QMF analysis and synthesis filters $h_{k'}(n)$ and $f_{k'}(n)$, respectively, are cosine-modulated versions of a real and linear-phase impulse response of the prototype filter $h(n)$, i.e., (39), shown at the bottom of the next page, where N is the number of FIR taps. Denote $H(z) = \sum_{n=0}^{N-1} h(n)z^{-n}$ as the z-transform of $h(n)$; the z-transforms of $h_{k'}(n)$ are

$$H^{(k')}(z) = \underbrace{a_{k'} c_{k'} H\left(zW^{(k+\frac{1}{2})}\right)}_{H^{(k',1)}(z)} + \underbrace{a_{k'}^* c_{k'}^* H\left(zW^{-(k'+\frac{1}{2})}\right)}_{H^{(k',2)}(z)} \quad (40)$$

where $W = e^{-j(\pi/M')}, \sqcup a_{k'} = e^{j\theta_{k'}}, \sqcup c_{k'} = W^{(k'+(1/2))((N-1)/2)}$, and $\theta_{k'} = (-1)^{k'}(\pi/4)$. Due to the mirror effect, the signal correlation is very low for a large k' and noninteger τ/T_S. Therefore, direct utilization of a QMF subband filter bank does not bring adequate signal correlation enhancement for different subbands. To solve this problem, we partition each subband analysis filter into two sub-subband filters $H^{(k',1)}(z)$ and $H^{(k',2)}(z)$. Consequently, in our modified QMF subband processing scheme, the analysis filter bank consists of $2M'$ subband coding (SBC) filter banks, while the synthesis filter bank consists of M' QMF banks.
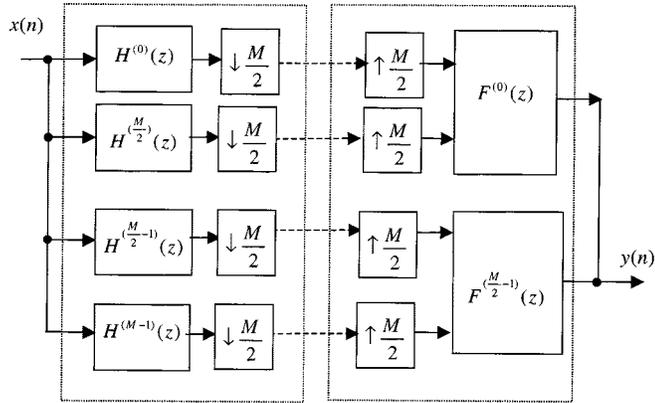
Fig. 8. Block diagram of a modified QMF bank.

To simplify and unify the notation, we let $M = 2M'$ and denote the subband index (k', i) into k so that

$$k = \begin{cases} k' & i = 1 \\ k' + M' & i = 2 \end{cases} \tag{41}$$

Then, we have (42) and (43), shown at the bottom of the page, where for the synthesis filters, $0 \le k < M/2$, since only $M/2$ filters are required. The kth subband ($k \ge M/2$) uses the same synthesis filter of the $(k - M/2)$th subband. Fig. 8 shows the configuration of the modified QMF bank.

Similar to (37), the autocorrelation functions of the outputs of these two sub-subband filters are obtained as (44), shown at the bottom of the page. Since $r^{(k+(M/2))}(0 \le k < M/2)$ is the conjugate of $r^{(k)}$, they have the same amplitude. From (44), it is seen that the signal correlation coefficient between two multipath ray components in kth two QMF sub-subband filter outputs is calculated by

$$\rho^{(k)}(\tau) = \alpha r^{(k)}(\tau)/r^{(k)}(0). \tag{45}$$

Fig. 9 shows the signal correlation coefficient for the different subbands. The FIR coefficients are computed based on [22], and the number of taps is 48, 64, 128, and 256 for $M = 4, 8, 16$, and 32, respectively. From the figure, it is clear that $|\rho^{(k)}(\tau)|$ is flat over the subbands except the minor degradation at the two sub-subbands of $k = (M/2) - 1$ and $k = M/2$ when τ/T_S is not an integer. Therefore, the signal correlation is almost equally enhanced for the different subbands after the subband signal processing based on modified-QMF banks.

The signal correlation coefficient is plotted as the dashed line in Fig. 6 for $B\tau = 1$ and $k = 0$. It is evident that the modified QMF-based filter banks have very close signal correlation enhancement performance to that of the ideal FIR filters.

In the above analysis, M is set depending on the signal correlation improvement and the requirement of subband processing. In practice, M should be chosen depending on the environment

$$\begin{cases} h_{k'}(n) = 2h(n)\cos\left((2k'+1)\dfrac{\pi}{2M'}\left(n - \dfrac{N-1}{2}\right) + (-1)^{k'}\dfrac{\pi}{4}\right) \\ f_{k'}(n) = 2h(n)\cos\left((2k'+1)\dfrac{\pi}{2M'}\left(n - \dfrac{N-1}{2}\right) - (-1)^{k'}\dfrac{\pi}{4}\right) \end{cases} \quad 0 \le n \le N-1, \quad 0 \le k' \le M'-1 \tag{39}$$

$$\begin{cases} H^{(k)}(z) = \begin{cases} a_k c_k H\left(zW^{(k+\frac{1}{2})}\right) & 0 \le k < \dfrac{M}{2} \\ a_{k-\frac{M}{2}}^* c_{k-\frac{M}{2}}^* H\left(zW^{-(k+\frac{1-M}{2})}\right) & \dfrac{M}{2} \le k < M \end{cases} \\ F^{(k)}(z) = a_k^* c_k H\left(zW^{(k+\frac{1}{2})}\right) + a_k c_k^* H\left(zW^{-(k+\frac{1}{2})}\right) & 0 \le k < \dfrac{M}{2} \end{cases} \tag{42}$$

$$\begin{cases} h_k(n) = \begin{cases} 2h(n)e^{(2k+1)\frac{\pi}{M}(n-\frac{N-1}{2})+(-1)^k\frac{\pi}{4}} & 0 \le k < \dfrac{M}{2} \\ 2h(n)e^{-(2k-M+1)\frac{\pi}{M}(n-\frac{N-1}{2})-(-1)^{(k-\frac{M}{2})}\frac{\pi}{4}} & \dfrac{M}{2} \le k < M \end{cases} \\ f_k(n) = 2h(n)\cos\left((2k+1)\dfrac{\pi}{M}\left(n - \dfrac{N-1}{2}\right) - (-1)^k\dfrac{\pi}{4}\right) & 0 \le k < \dfrac{M}{2} \end{cases} \tag{43}$$

$$r^{(k)}(\tau) = \begin{cases} \displaystyle\sum_{n=0}^{N-1}\sum_{m=0}^{N-1} h(n)h(m)e^{-j(2k+1)(n-m)} r\left(\tau - \dfrac{n-m}{B}\right) & 0 \le k < \dfrac{M}{2} \\ \displaystyle\sum_{n=0}^{N-1}\sum_{m=0}^{N-1} h(n)h(m)W^{j(2k+1-M)(n-m)} r\left(\tau - \dfrac{n-m}{B}\right) & \dfrac{M}{2} \le k < M \end{cases} \tag{44}$$
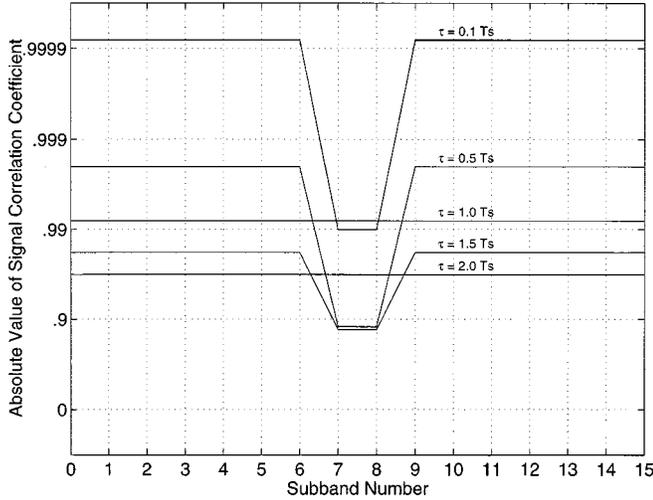
Fig. 9. Signal correlation coefficient of modified QMF banks at the different subbands ($M = 16$).

coherence bandwidth [23] as well as the employed signal bandwidth.

IV. SUBBAND ADAPTIVE ARRAY

In the above sections, we discussed the enhancement of the signal correlation between multipath rays via subband signal processing using filter banks. Applying the subband signal-processing technique to adaptive arrays forms subband adaptive arrays, which implement space–time processing for effective mitigation of both CCI and ISI problems in a multipath fading environment.

We consider an adaptive array with the modified pseudo-QMF filter banks, implementing the Wiener–Hopf solution. The analysis is presented in terms of optimum weight vectors and exact statistics with no specific adaptive algorithm being considered.

The output signal of each array sensor and the reference signal are divided into M subbands, respectively. Therefore, the steady-state optimum weight vector of the kth subband, under the MMSE criterion, is given by

$$\mathbf{w}^{(k)} = \mathbf{R}_{XX}^{(k)-1}\mathbf{r}_D^{(k)} \quad k = 1,\ldots,M \quad (46)$$

where

$$\mathbf{R}_{XX}^{(k)} = E\left[\mathbf{x}^{(k)}(t)\mathbf{x}^{(k)H}(t)\right] \quad (47)$$

$$\mathbf{r}_D^{(k)} = E\left[\mathbf{x}^{(k)}(t)r^{(k)*}(t)\right]. \quad (48)$$

From the discussion of Sections II and III, the multipath rays in each subband become highly correlated. As a result, they asymptotically behave like a single ray as M increases.

From (8) and (12), the array output signal-to-interference-plus-noise ratio (SINR) without subband signal processing is given by

$$\text{SINR}_0 = \frac{P_{S0}}{P_{IN0}} = \frac{E\{|\mathbf{w}^H\tilde{s}_D(t)\tilde{\mathbf{a}}_D|^2\}}{E\{\mathbf{w}^H\mathbf{R}_N\mathbf{w}\}}$$

$$= \frac{\sigma_D^2|\tilde{\mathbf{a}}_D^H\mathbf{R}_N^{-1}\tilde{\mathbf{a}}_D|^2}{\tilde{\mathbf{a}}_D^H\mathbf{R}_N^{-1}\mathbf{R}_N\mathbf{R}_N^{-1}\tilde{\mathbf{a}}_D} = \sigma_D^2\tilde{\mathbf{a}}_D^H\mathbf{R}_N^{-1}\tilde{\mathbf{a}}_D \quad (49)$$

where P_{S0} and P_{IN0} are the SOI output power and the output interfering signal power, respectively. With subband signal processing, the SOI output power $P_S^{(k)}$ and the output interfering signal power $P_{IN}^{(k)}$ at the kth subband are given by

$$P_S^{(k)} = \sigma_D^{(k)2}\left|\mathbf{w}^{(k)H}\tilde{\mathbf{a}}_D^{(k)}\right|^2$$

$$= \sigma_D^{(k)2}\left(\tilde{\mathbf{a}}_D^{(k)H}\mathbf{R}_{XX}^{(k)-1}\tilde{\mathbf{a}}_D^{(k)}\right)^2$$

$$= g^{(k)2}\sigma_D^{(k)2}\left(\tilde{\mathbf{a}}_D^{(k)H}\mathbf{R}_N^{(k)-1}\tilde{\mathbf{a}}_D^{(k)}\right)^2 \quad (50)$$

$$P_{IN}^{(k)} = \mathbf{w}^{(k)H}\mathbf{R}_N^{(k)}\mathbf{w}^{(k)}$$

$$= \sigma_D^{(k)2}\tilde{\mathbf{a}}_D^{(k)H}\mathbf{R}_{XX}^{(k)-1}\mathbf{R}_N^{(k)}\mathbf{R}_{XX}^{(k)-1}\tilde{\mathbf{a}}_D^{(k)}$$

$$= g^{(k)2}\sigma_D^{(k)2}\tilde{\mathbf{a}}_D^{(k)H}\mathbf{R}_N^{(k)-1}\tilde{\mathbf{a}}_D^{(k)} \quad (51)$$

where

$$g^{(k)} = \sigma_D^{(k)2}\left(1 - \sigma_D^{(k)2}\tilde{\mathbf{a}}_D^{(k)H}\mathbf{R}_{XX}^{(k)-1}\tilde{\mathbf{a}}_D^{(k)}\right). \quad (52)$$

The output SINR of a subband adaptive array is expressed as

$$\text{SINR}_{SUB} = \frac{\sum_{k=0}^{M-1}P_S^{(k)}}{\sum_{k=0}^{M-1}P_{IN}^{(k)}}$$

$$= \frac{\sum_{k=0}^{M-1}g^{(k)2}\sigma_D^{(k)2}\left|\tilde{\mathbf{a}}_D^{(k)H}\mathbf{R}_N^{(k)-1}\tilde{\mathbf{a}}_D^{(k)}\right|^2}{\sum_{k=0}^{M-1}g^{(k)2}\tilde{\mathbf{a}}_D^{(k)H}\mathbf{R}_N^{(k)-1}\tilde{\mathbf{a}}_D^{(k)}}. \quad (53)$$

The SINR improvement by subband array processing is most significant in the following cases.

In the first case, the number of DOFs is less than the total number of rays but is larger than the total number of the desired and CCI sources, while the signal correlation between the multipath rays of each of source is small. Consider a mobile station at high-speed digital communications environment. Although the number of CCI signals is limited, they can arrive with a large number of multipath rays with low signal correlation. In this case, the conventional adaptive array cannot effectively suppress the CCI rays as well as the interfering multipath rays of the desired signal. A subband adaptive array, on the other hand, can suppress the CCI rays and combine the multipath rays of the desired signal. By applying subband array techniques with sufficient number of subbands, as discussed in Section II, the subbands become narrow enough so that the multipath rays of each signal become highly correlated. In this case, the ISI component of the desired signal is negligible, and the multipath rays of a CCI signal becomes effectively rank one and can be removed by a single DOF.

In the second case, the multipath rays of the desired signal come from a small angular sector so that it is not possible for a conventional adaptive array to suppress the interfering multipath while maintaining the proper gain of the desired signal. A subband adaptive array is not sensitive to this problem. In a subband array, the ISI component can be reduced with sufficient number of subbands such that it is not necessary for the array to suppress the multipath rays.

V. SIMULATIONS

Computer simulations are performed to support our analysis. A three-element uniform linear array with half-wavelength spacing is considered. The sample matrix inversion (SMI)
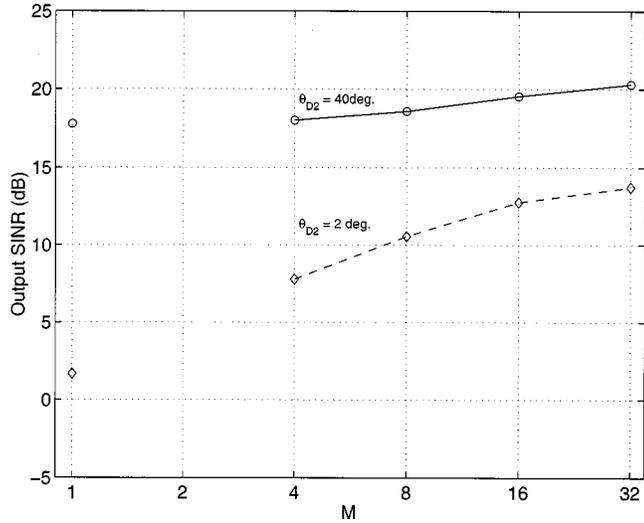
Fig. 10. Output SINR versus M ($\sigma_{D1}^2 = \sigma_{D2}^2 = 10$ dB, $\theta_{D1} = 0°$, $\tau = T_S$).

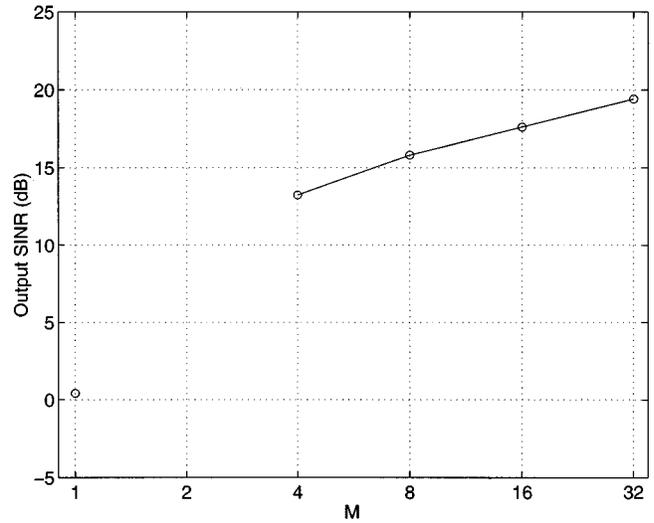
Fig. 11. Output SINR versus M ($\sigma_{D1}^2 = \sigma_{D2}^2 = \sigma_{D3}^2 = \sigma_{D4}^2 = 10$ dB, $\theta_{D1} = 0°$, $\theta_{D2} = 20°$, $\theta_{D3} = -20°$, $\theta_{D4} = -60°$, $\tau_2 = T_S, \tau_3 = 2T_S, \tau_4 = 3T_S$).

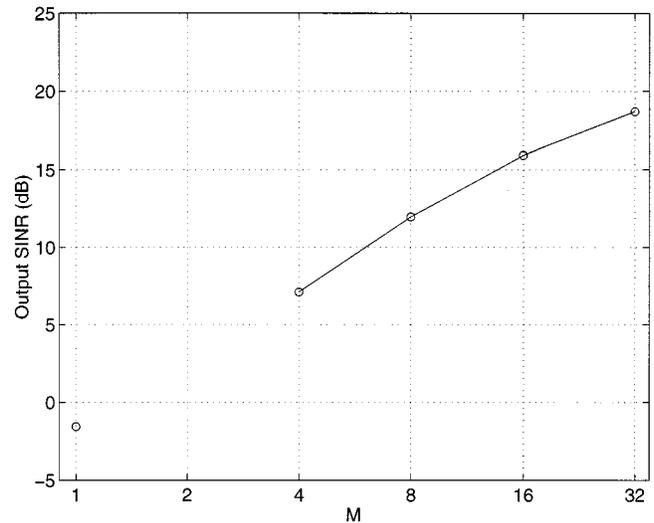

Fig. 12. Output SINR versus M ($\sigma_{D1}^2 = \sigma_{D2}^2 = 10$ dB, $\theta_{D1} = 0°$, $\theta_{D2} = 20°$, $\tau_D = T_S$, $\sigma_{I1}^2 = \sigma_{I2}^2 = 20$ dB, $\theta_{I1} = -20°$, $\theta_{I2} = -60°$, $\tau_I = T_S$).

method [24] is used to approximate the optimum weights in obtaining the weight vector and the output SINR. The bit error rate (BER) is evaluated by numerical simulations using the optimum weight vector. Both the desired signal and the interference signals are considered with quadrature phase-shift keying modulation, and the rolloff rate is 0.5.

We first consider the case where only the desired signal with two rays is present. It is assumed that $\sigma_{D1}^2 = \sigma_{D2}^2 = 10$ dB and $\sigma_N^2 = 0$ dB. Fig. 10 shows the output SINR versus the number of subbands[1] M. In Fig. 10, the direction of arrival (DOA) of the direct ray is $0°$ from the broadside direction. We show two cases where the DOA of the delayed ray is $40°$ and $2°$, respectively. The time delay between the two rays is T_S, so that the two rays are uncorrelated.

For the case of $\theta_{D2} = 40°$, the two rays are widely separated in angle. With two DOFs, the uncorrelated delayed ray is suppressed, leading to a high output SINR, even when no subband signal processing is performed. Thus, the improvement by subband signal processing is not significant. However, for the case of $\theta_{D2} = 2°$, the output SINR is very low (1.7 dB) without subband processing. The degradation of the output SINR is caused by the resolution limitation of the array since the two signals are closely separated. The array output SINR performance is improved rapidly as M increases, which confirms the equalization effectiveness of subband signal processing.

Next, we add two additional multipath rays to the previous example, creating a desired signal with three copies. The corresponding array output SINR is shown in Fig. 11. The two additional multipath rays are of equal power with DOAs of $-20°$ and $-60°$, and their delay times relative to the direct ray are $2T_S$ and $3T_S$, respectively. In this case, when no subband signal processing is performed, the four rays are uncorrelated to each other, and the array will attempt to suppress the three delayed rays. We note that the three-element array only has two DOFs. Therefore, the array DOFs are not sufficient, and the array cannot provide good performance. It is clear from

Fig. 11 that the output SINR is near 0 dB. On the other hand, when subband signal processing is performed, the four rays will asymptotically behave as an equivalent ray, and the output SINR increases rapidly as M increases. The output SINR exceeds 13 dB when $M = 4$ or larger, and the BER is lower than 10^{-5}.

Fig. 12 depicts the output SINR when two CCI signals are added to the case considered in Fig. 10. The powers of the CCI rays are $\sigma_{I1}^2 = \sigma_{I2}^2 = 20$ dB. Their DOAs are $-20°$ and $-60°$, respectively, and the time delay between the two rays equals to T_S. When no subband signal processing is performed, the array will strive to suppress the delayed ray of the desired signal and the two uncorrelated CCI rays. Similar to the case in Fig. 11, the number of DOFs is not sufficient to achieve this task. The result is a very poor output SINR, as low as -1.6 dB. When subband signal processing is performed, the two rays
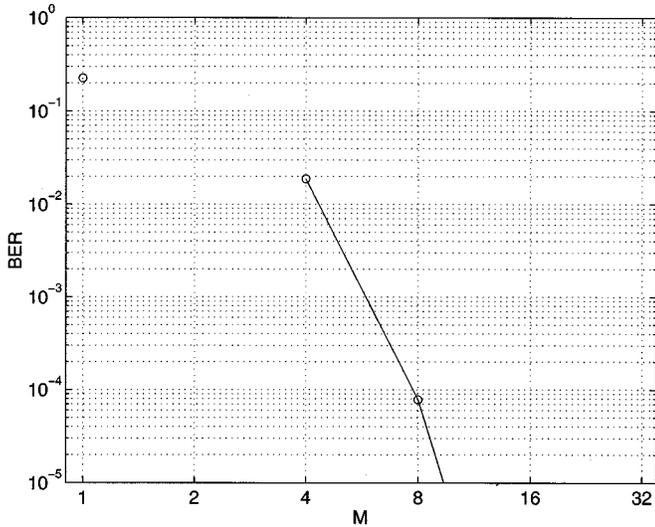
[1]In the figures, $M = 1$ denotes the case where the signal is processed without subband decomposition.

Fig. 13. BER versus M ($\sigma_{D1}^2 = \sigma_{D2}^2 = 10$ dB, $\theta_{D1} = 0°$, $\theta_{D2} = 20°$, $\tau_D = T_S$, $\sigma_{I1}^2 = \sigma_{I2}^2 = 20$ dB, $\theta_{I1} = -20°$, $\theta_{I2} = -60°$, $\tau_I = T_S$).

of the desired signal will be treated as an equivalent single one, and those of the CCI as another equivalent ray. Thus, the array DOFs will be sufficient, and the output SINR increases to 7.1 dB for $M = 4$ and 12 dB for $M = 8$. The corresponding BER performance is shown in Fig. 13, which decreases rapidly as M increases. Fig. 14 shows the original waveform received at the first array sensor with the ISI and CCI components before the subband array processing and the waveform of the subband array output.

To examine the effect of longer time delay on the required number of subbands, we consider a similar scenario as that discussed in Fig. 12, where the time delay between the two rays of the desired signal is assumed to be $4T_S$. The time delay between the two rays of the CCI signal is also set to $4T_S$. Fig. 15 shows the output SINR versus the number of subbands M. It is evident from this figure that the output SINR does not improve when M is small ($M \leq 4$). About four times of the number of subbands in the case discussed in Fig. 12 should be used to achieve the same output SINR performance.

VI. CONCLUSION

We have proposed subband adaptive arrays for multipath fading mitigation in wireless communications. It has been shown that subband adaptive arrays, which provide suboptimal frequency-spatial signal processing, are very effective both in mitigating the intersymbol interference problem caused by frequency-selective fading and in suppressing the cochannel interference signals in mobile communications.

The performance of the adaptive array in the presence of multipath rays has been analyzed. We have shown that these rays can be considered as a single path when the signal correlation between the rays is high. The analysis of the signal correlation enhancement between the multipath rays by subband signal processing was presented. We have discussed the signal correlation enhancement performance for filter banks using ideal filters, DFT, and modified QMF filters. The impressive performance of
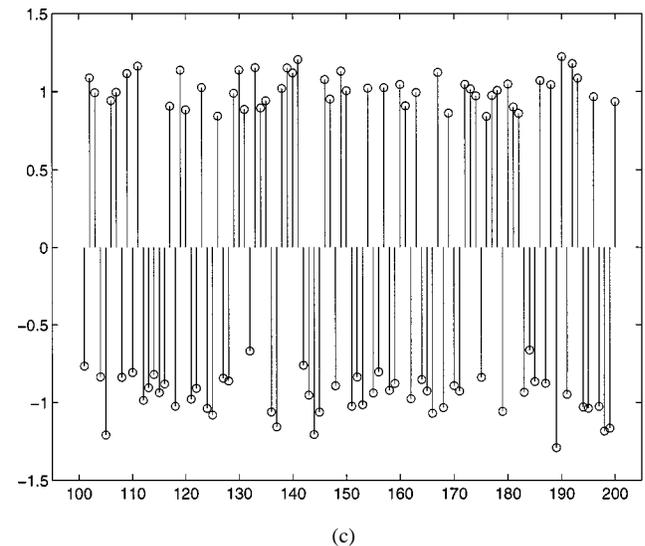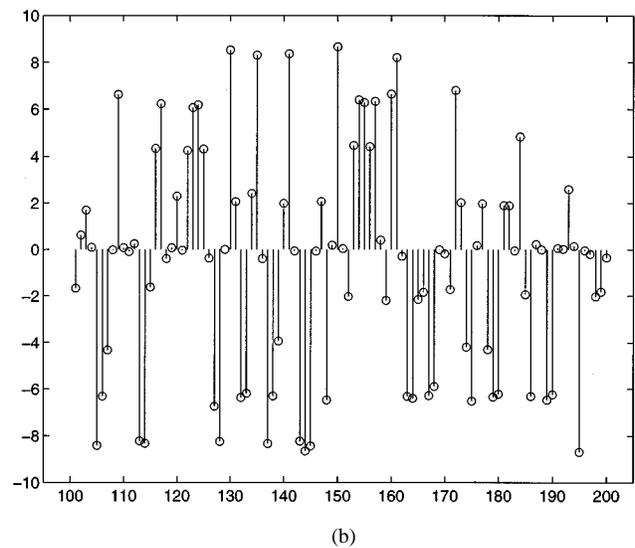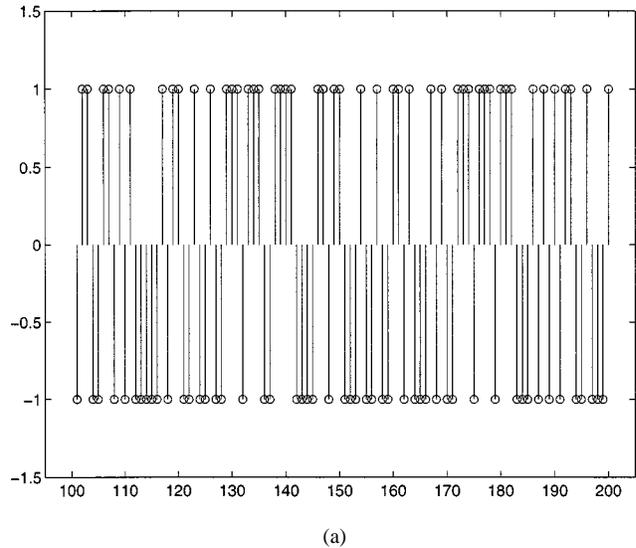

(a)

(b)

(c)

Fig. 14. Waveforms for 100 symbols before and after subband processing ($\sigma_{D1}^2 = \sigma_{D2}^2 = 10$ dB, $\theta_{D1} = 0°$, $\theta_{D2} = 20°$, $\tau_D = T_S$, $\sigma_{I1}^2 = \sigma_{I2}^2 = 20$ dB, $\theta_{I1} = -20°$, $\theta_{I2} = -60°$, $\tau_I = T_S$). (a) Waveform of the original desired signal. (b) Signal waveform received at the first sensor. (c) Signal waveform of the subband array output.
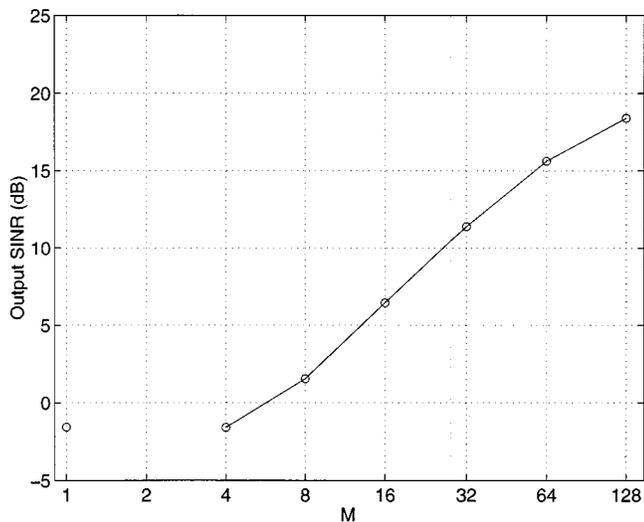
Fig. 15. Output SINR versus M ($\sigma_{D1}^2 = \sigma_{D2}^2 = 10$ dB, $\theta_{D1} = 0°$, $\theta_{D2} = 20°$, $\tau_D = 4T_S$, $\sigma_{I1}^2 = \sigma_{I2}^2 = 20$ dB, $\theta_{I1} = -20°$, $\theta_{I2} = -60°$, $\tau_I = 4T_S$).

modified QMF banks, which are practical to use, is also demonstrated. The simulation results confirmed the analyses and the effectiveness of the proposed method to combat the multipath fading for both the desired and cochannel interference signals.

ACKNOWLEDGMENT

REFERENCES

[1] Y. Ogawa, M. Ohmiya, and K. Itoh, "An LMS adaptive array for multipath fading reduction," *IEEE Trans. Aerosp. Electron. Syst.*, vol. AES-23, pp. 17–23, Jan. 1987.

[2] S. Anderson, M. Millnert, M. Viberg, and B. Wahlberg, "An adaptive array for mobile communication systems," *IEEE Trans. Veh. Technol.*, vol. 40, pp. 230–236, 1991.

[3] Y. Zhang, "Multipath fading equalization by an adaptive array," in *Proc. Int. Symp. Antennas Propagat.*, Sapporo, Aug. 1992, pp. 149–152.

[4] N. Ishii and R. Kohno, "Spatial and temporal equalization based on an adaptive tapped-delay-line array antenna," *IEICE Trans. Commun.*, vol. E78-B, no. 8, pp. 1162–1169, Aug. 1995.

[5] Y. Doi, T. Ohgane, and E. Ogawa, "ISI and CCI canceller combining the adaptive array antennas and the Viterbi equalizer in a digital mobile radio," in *Proc. IEEE VTC*, pp. 81–85, Apr. 1996.

[6] T. A. Thomas and M. D. Zoltowski, "Novel receiver signal processing for interference calcellation and equalization in cellular TDMA communications," in *Proc. ICASSP*, 1997, pp. 3881–3884.

[7] J.-W. Liang and A. Paulraj, "Two stage CCI/ISI reduction with space-time processing in TDMA cellular networks," in *Proc. 30th Annual Asilomar Conf. on Signals, Systems, and Computers*, Pacific Grove, CA, Nov. 1996.

[8] A. J. Paulraj and C. B. Papadias, "Space-time processing for wireless communications," *IEEE Signal Processing Mag.*, vol. 14, pp. 49–83, Nov. 1997.

[9] Y. Zhang, K. Yang, and M. G. Amin, "Performance analysis of subband adaptive arrays in multipath propagation environment," in *Proc. IEEE Workshop Statistical Signal and Array Signal Processing*, Portland, OR, Sept. 1998, pp. 17–20.

[10] N. J. Fliege, *Multirate Digital Signal Processing*. New York: Wiley, 1994.

[11] Y. Zhang, K. Yang, and M. G. Amin, "Adaptive subband arrays for multipath fading mitigation," in *Proc. IEEE AP-S Int. Symp.*, Atlanta, GA, June 1998, pp. 380–383.

[12] Y. Zhang, K. Yang, and Y. Karasawa, "Subband CMA adaptive arrays in multipath fading environment," *IEICE Trans. Commun.*, vol. J82-B, no. 1, pp. 97–108, Jan. 1999.

[13] T. Sekiguchi and Y. Karasawa, "CMA adaptive array antennas using analysis and synthesis filter banks," *IEICE Trans. Fund.*, vol. E81-A, no. 8, pp. 1570–1577, Aug. 1998.

[14] F. Lorenzelli, A. Wang, D. Korompis, R. Hydson, and K. Yao, "Optimization and performance of broadband microphone arrays," in *Proc. SPIE*, vol. 2563, July 1995, pp. 158–169.

[15] J. M. Khalab and M. K. Ibrahim, "Novel multirate adaptive beamforming technique," *Electron. Lett.*, vol. 30, no. 15, pp. 1194–1195, 1994.

[16] H. Wang and M. Kaveh, "Coherent signal subspace processing for the detection and estimation of angles of arrival of multiple wideband sources," *IEEE Trans. Acoust., Speech, Signal Processing*, vol. 33, pp. 823–831, Aug. 1985.

[17] M. G. Amin, "High resolution direction of arrival estimation of multiple wide-band sources in multichannel adaptive nulling systems," in *Proc. ICASSP*, Atlanta, GA, May 1996.

[18] J. Yang and A. Swindlehurst, "Maximum SINR beamforming for correlated sources," in *Proc. ICASSP*, Detroit, MI, May 1995, pp. 1916–1919.

[19] I. J. Gupta, "Effect of jammer power on the performance of adaptive arrays," *IEEE Trans. Antennas Propagat.*, vol. AP-32, Sept. 1984.

[20] J. E. Hudson, *Adaptive Array Principles*. New York: Peregrinus, 1989.

[21] R. D. Koipillai and P. P. Vaidyanathan, "New results of cosine-modulated FIR filter banks satisfying perfect reconstruction," in *Proc. ICASSP*, Toronto, ON, Canada, May 1991, pp. 1789–1792.

[22] T. Q. Nguyen, "Near-perfect-reconstruction pseudo-QMF banks," *IEEE Trans. Signal Processing*, vol. 42, pp. 65–76, 1994.

[23] W. C. Y. Lee, *Mobile Communications Design Fundamentals*, 2nd ed. New York: Wiley, 1993.

[24] I. S. Reed, J. D. Mallet, and L. E. Brennan, "Rapid convergence rate in adaptive arrays," *IEEE Trans. Aerosp. Electron. Syst.*, vol. AES-10, pp. 853–863, Nov. 1974.

Yimin Zhang (M'88) received the M.S. and Ph.D. degrees from the University of Tsukuba, Japan, in 1985 and 1988, respectively.

He joined the Faculty of the Department of Radio Engineering, Southeast University, China, in 1988. He was a Technical Manager with Communication Laboratory Japan in 1995–1997 and a Visiting Researcher at ATR Adaptive Communications Research Laboratories, Japan, in 1997–1998. Currently, he is a Research Associate in the Department of Electrical and Computer Engineering, Villanova University, Villanova, PA. His current research interests are in the areas of array signal processing, space-time adaptive processing, blind signal processing, digital mobile communications, and time-frequency analysis.

Kehu Yang (M'99) received the B.E., M.S., and Ph.D. degrees from Xidian University (formerly the Northwest Telecommunication Engineering Institute), Xi'an, China, in 1982, 1984, and 1995, respectively.

He joined Xidian University in 1985, where he became an Associate Professor in 1996. Since December 1998, he has been a Visiting Researcher at ATR Adaptive Communications Research Laboratories, Kyoto, Japan. His research interests include array signal processing, space–time adaptive processing, and space–time multiuser detection for mobile communications.

Moeness G. Amin (S'82–M'83–SM'91–F'00) received the Ph.D. degree in electrical engineering from University of Colorado, Boulder, in 1984.

He has been on the Faculty of the Department of Electrical and Computer Engineering, Villanova University, Villanova, PA, since 1985, where is now a Professor. He serves on the Committee of Arts and Science of the Franklin Institute. His current research interests are in the areas of time–frequency analysis, spread-spectrum communications, smart antennas, and blind signal processing.

Dr. Amin received the 1997 IEEE Philadelphia Section Service Award and the IEEE Third Millennium Medal. From 1995 to 1997, he was an Associate Editor of the IEEE TRANSACTIONS ON SIGNAL PROCESSING and a member of the Technical Committee of the IEEE Signal Processing Society on Statistical Signal and Array Processing. He is currently a member of the IEEE Signal Processing Society Technical Committee on Signal Processing for Communications. He was the General Chair of the 1994 IEEE International Symposium on Time-Frequency and Time-Scale Analysis. He is the General Chair of the 2000 IEEE Workshop on Statistical Signal and Array Processing. He received the 1997 Villanova University Outstanding Faculty Research Award.